Density Functional Theory for Charge Transfer: The Nature of the N-Bands of Porphyrins and Chlorophylls Revealed through CAM-B3LYP, CASPT2, and SAC-CI Calculations

Zheng-Li Cai,[†] Maxwell J. Crossley,[†] Jeffrey R. Reimers,*[,†] Rika Kobayashi,[‡] and Roger D. Amos[‡,§]

School of Chemistry, The University of Sydney, Sydney, New South Wales 2006, Australia, and Supercomputer Facility and Research School of Chemistry, The Australian National University, Canberra, ACT 2600, Australia

Received: June 1, 2006

While density functional theory (DFT) has been proven to be extremely useful for the prediction of thermodynamic and spectroscopic properties of molecules, to date most functionals used in common implementations of DFT display a systematic failure to predict the properties of charge-transfer processes. While this is explicitly manifest in Rydberg transitions of atoms and molecules and in molecular charge-transfer spectroscopy, it also becomes critical for systems containing extended conjugation such as polyenes and other conducting polymers, porphyrins, chlorophylls, etc. A new density functional, a Coulomb-attenuated hybrid exchange-correlation functional (CAM-B3LYP), has recently been developed specifically to overcome these limitations, and it has been shown to properly predict molecular charge-transfer spectra. Here, we demonstrate that it predicts qualitatively reasonable spectra for porphyrin, some oligoporphyrins, and chlorophyll. However, alternate density functionals developed to overcome the same limitations such as current-density functional theory are shown, in their present implementation, to remain inadequate. The CAM-B3LYP results are shown to be in excellent agreement with complete-active-space plus second-order Møller−Plesset perturbation theory and symmetry-adapted cluster configuration interaction calculations: These depict the N and higher bands of porphyrins and chlorophylls as being charge-transfer bands associated with localization of molecular orbitals on individual pyrrole rings. The validity of the basic Gouterman model for the spectra of porphyrins and chlorophylls is confirmed, rejecting modern suggestions that non-Gouterman transitions lie close in energy to the Q-bands of chlorophylls. As porphyrins and chlorophylls provide useful paradigms for problems involving extended conjugation, the results obtained suggest that many significant areas of nanotechnology and biotechnology may now be realistically treated by cost-effective density-functional-based computational methods.

1. Introduction

Density functional theory (DFT) provides an efficient method for the a priori prediction of the properties of both molecular and solid-state systems, and in particular time-dependent DFT (TD-DFT) has been shown to be reliable for the prediction of excited-state properties.[1−7] However, the functionals currently used in DFT calculations are well-known to provide erratic treatment of molecular processes involving molecular charge transfer[1,8] including Rydberg transitions,[1,4,5,9−11] the excited states of porphyrins[12] and chlorophylls,[13] and the properties of conducting polymer prototypes such as polyacetylene.[12] Errors of many orders of magnitude are also produced by modern functionals for the hyperpolarizabilities of polyenes and other systems showing extended conjugation,[14−16] again due to the improper representation of charge-transfer processes in these systems. Indeed, traditional density functionals predict that either polyacetylene is a metal or that its ground state is paramagnetic.[12] These weaknesses significantly reduce the applicability of computationally efficient a priori computational methods in nanotechnological applications involving conducting polymers, molecule−metal as well as molecule−semiconductor junctions, through-molecule electron transfer, exciton transport, and primary charge separation in both natural photosynthetic organisms and artificial molecular solar cells, conducting wires, and molecular electronic devices.[17]

The failure of traditional functionals to properly treat charge transfer has been associated with incorrect asymptotic forms of the exchange-correlation potential,[6,10,18−20] an error that is manifested whenever an electron is moved a large distance but not completely removed from the system. A variety of approaches have been considered to treat this problem including external asymptotic corrections,[10,21,22] modified functionals,[19,20,23] and inclusion of functionals of the current density.[24] Here, we consider two very recent proposals: the current-density functional (CDFT) of van Faassen, de Boeij, van Leeuwen, Berger, and Snijders[24] and the CAM-B3LYP functional of Yanai, Tew, and Handy[25] based on the long-range correction of the exchange potential introduced by Tawada et al.[20] applied to modify the B3LYP[26,27] functional. Through the incorporation of functionals of both the current density and the charge density into Kohn−Sham approaches, CDFT seeks to provide a good description of long-range interactions along with the usually well-treated atomic-range interactions, with the hope that charge-

* Author to whom correspondence should be addressed. E-mail: reimers@chem.usyd.edu.au.
[†] The University of Sydney.
[‡] Supercomputer Facility, The Australian National University.
[§] Research School of Chemistry, The Australian National University.

10.1021/jp063376t CCC: $33.50
Published on Web 07/18/2006

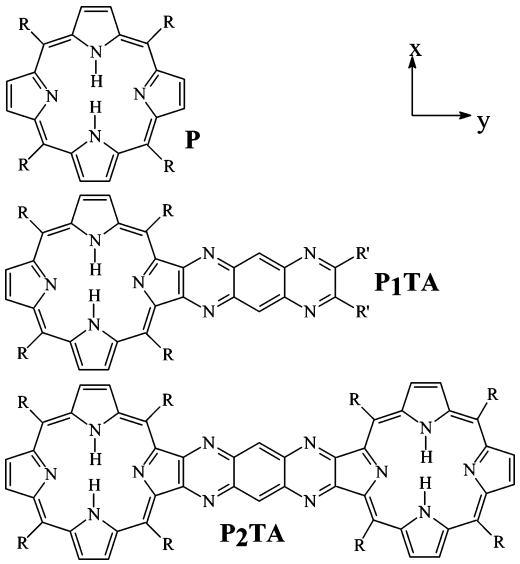

Figure 1. Chemical structures of P, P_1TA, and P_2T. R = H in calculations; R = H or 3,5-di-*tert*-butylphenyl in experiments. The in-plane molecular axis directions are also indicated.

transfer processes on the intermediate molecular length scale may be adequately described. It has been demonstrated to provide good results for small conjugated molecules and some conjugated polymers,[24,28] though Ullrich and Burke[29] have pointed out that the functional used can be expected to fail in some circumstances. CAM-B3LYP has been demonstrated to provide good results for Rydberg transitions and excitations in small molecules[20,30] as well as for intermolecular charge-transfer transitions.[20] It has also been successfully applied to the charge-transfer excitations in the zincbacteriochlorin−bacteriochlorin complex.[31] Here, we consider the application of these methods to some extended porphyrins shown in Figure 1 and to chlorophyll (Chl) a, molecules of considerable importance in nanotechnology and biotechnology. We also consider older functionals such as B3LYP itself[26,27] and SAOP[23] designed to increase the Kohn−Sham band gap in DFT calculations of small molecules and for reference some traditional generalized-gradient-approximation (GGA) functionals including BP86[32,33] and PW91,[34] whose failure to adequately describe porphyrins, chlorophylls, and conjugated polymers is well established.[12,13]

The spectroscopy of porphyrins is usually interpreted in terms of the four-orbital Gouterman model[35,36] depicting two low-energy near-degenerate pseudo-forbidden transitions known as the Q-bands and two extremely intense and narrow high-energy transitions known as the B or Soret bands. The components of these systems are labeled Q_x, Q_y, B_x, and B_y after their polarization directions in the (x,y) planes of the macrocyclic systems. For chlorophylls, the situation is very similar except that, because of the reduced symmetry, the Q_y band becomes very intense. All calculations performed using ab initio configuration interaction expansions of the molecular electronic structure based on Hartree−Fock reference wave functions vindicate the Gouterman model for porphyrins and chlorophylls, depicting in addition higher-energy transitions known as the N, L, etc. bands, bands that do correspond to weak observed absorption features;[37−48] the observed spectrum for porphyrin and its standard assignment are shown in Figure 2.

However, results obtained previously using traditional density functionals for porphyrins and chlorophylls have offered a significantly different picture of the spectroscopy in which the Gouterman transitions are embellished and/or swamped by a significant number of other bands.[12] For free-base porphyrin itself, one set of additional bands is usually predicted, at about the expected energy of the Soret bands. As a result, these bands have often been interpreted as being the Soret bands,[3,49] but herein we demonstrate that they are in fact the N-bands and are of strong charge-transfer character; the actual Soret bands are predicted to be much higher in energy, as shown in Figure 2. Although there is no experimental evidence to support the presence of non-Gouterman transitions between the Q and Soret bands in free-base porphyrin, such bands clearly appear in the spectra of the oligoporphyrins shown in Figure 2. However, as the figure indicates, traditional DFT methods predict a multitude of additional electronic states for these molecules and fail to capture the primary qualitative features of the excited-state manifolds;[12] alternatively, Hartree−Fock-based computational methods continue to provide qualitatively realistic predictions that can be used to assign the new features found in the experimental spectra.[38]

For chlorophylls the situation has not been so clear-cut. There has been no authoritative assignment of the observed spectrum of Chl a, with in particular two viable options appearing for the assignment of the weak Q_x band in the region between the intense Q_y origin and the Soret bands.[50−52] The possibility thus arises that an additional electronic origin to Q_x lies either very close to Q_y or midway between it and the Soret bands. As DFT calculations predict the appearance of non-Gouterman states in this region, novel reinterpretations of chlorophyll spectroscopy are possible.[53,54] However, Dreuw, Fleming, and Head-Gordon[55] have shown that the non-Gouterman states predicted by DFT have charge-transfer character, and Dahlbom and Reimers[13] using a fully DFT-optimized structure[56] for photosystem-1 (PS1) have shown that under physiological conditions the prevailing electric-field strengths would be sufficient to make a DFT-predicted non-Gouterman state the lowest-energy singlet excited state and hence dominate plant photophysics, in clear contradiction to experimental results. The B3LYP functional does not show such dramatic effects for bacteriochlorophyll,[57] however, but it is known to do so in a similar way for porphyrin.[12]

Fundamental questions remain as to the nature of non-Gouterman transitions in porphyrins and chlorophylls. Calculation methods that reproduce the major known qualitative features can be of considerable use in resolving these issues. Besides calculations performed using traditional DFT methods such as B3LYP and the new DFT methods CAM-B3LYP and CDFT, we also perform calculations using the Hartree−Fock-based complete-active-space plus second-order Møller−Plesset perturbation theory (CASPT2; perturbative) and symmetry-adapted cluster configuration interaction (SAC-CI; coupled-cluster) approaches. We isolate spectral feature predictions that are consistent across all qualitatively reasonable methods, determining the role played by charge-transfer transitions in these systems. This facilitates, for the first time, the identification of the intrinsic nature of the N-bands and the cause of their sensitivity to chemical environment.

2. Methods

Calculations are performed for Chl a, free-base porphyrin (P), free-base porphyrin with a fused tetraazaanthracene (P_1TA),[38] and the related oligoporphyrin dimer (P_2TA),[38] all shown in Figure 1. Note that, except for calibration purposes, the experimental results are for the tetrameso derivatives indicated in the figure while the calculations are performed on unsubstituted porphyrins. All excited-state properties evaluated from density functionals are obtained using the TD-DFT formalism. The ADF package[58,59] is used for all calculations for the CDFT[24]

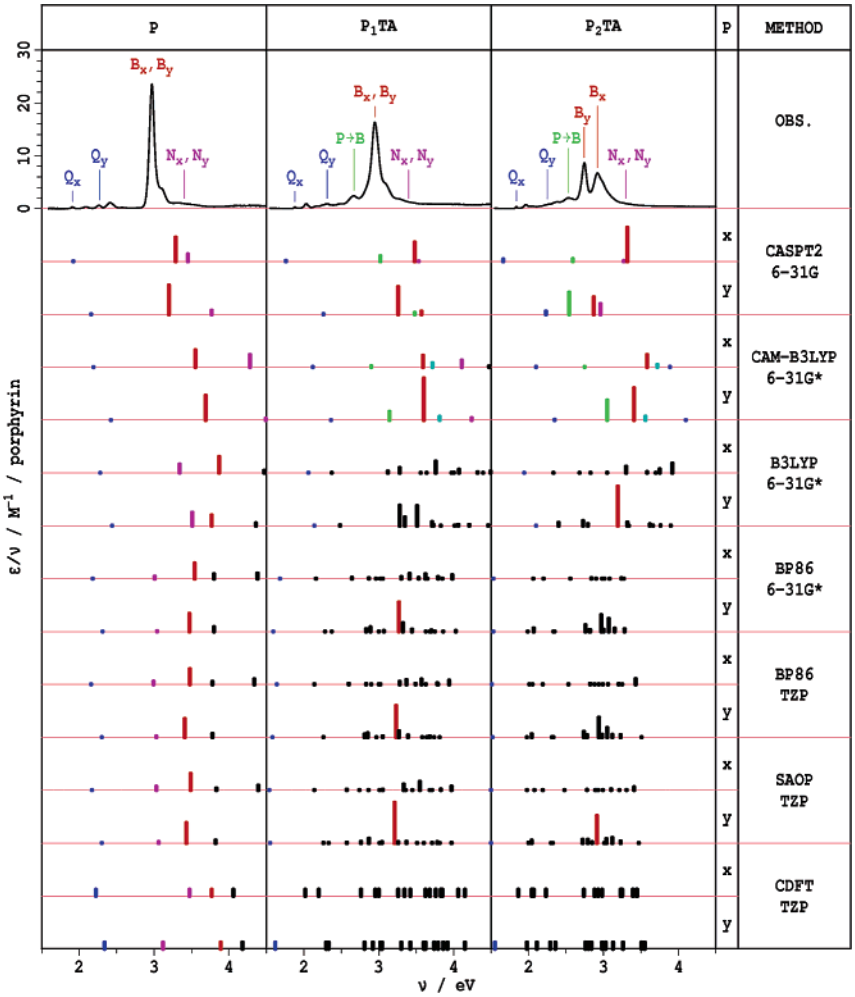

Figure 2. Observed (in light petroleum) and calculated (in the gas phase) electronic absorption spectra for P, P_1TA, and P_2TA: Q-bands in blue (both the usual intramolecular bands and high-energy inter-porphyrin charge transfer for P_2TA), Soret bands in red, N-bands in purple, porphyrin-to-bridge charge-transfer bands in green, bridge-to-porphyrin charge-transfer bands in cyan, and other bands (typically charge transfer) in black. No intensity information is available for CDFT.

and SAOP[23] functionals using the (extensive) TZP basis set, while all calculations for the CAM-B3LYP[25] and B3LYP[26,27] functionals are performed using the Development Version of Gaussian[60] (into which CAM-B3LYP has been coded)[31] using the 6-31G* basis set. To determine the effects of the two different basis sets used in these calculations, additional calculations for the BP86[32,33] density functional are performed using both methods. The CASPT2 calculations were performed by MOLCAS[61] using the 6-31G basis set. Coupled-cluster SAC-CI[62] calculations were performed using Gaussian with the 6-31G* basis set at zero field and the 6-31G basis set at finite field. All geometries used were obtained by optimization at the B3LYP/6-31G* level. The natures of the excited electronic states were determined by the application of applied electric fields up to 24 MV cm^{-1} in the in-plane directions; charge-transfer bands interact strongly with fields of this magnitude while the molecular Gouterman Q and Soret bands[35] of the porphyrins and chlorophylls do not.[13]

Application of all DFT-based methods is straightforward; the only extra parameter that must be entered is the number of excited electronic states required. Typically up to 20 excited states are determined. The excitation energies are found by the algorithm of Stratmann et al..[63] Similar search spaces are also required for the Hartree−Fock-based methods used, but additional parameters are also required.

For SAC-CI, a frozen 1s core was used, with the accuracy set to "levelone" (lowest available), the maximum number of "R2 operators" set to 2×10^7, and the maximum number of "general R" operators set to 5×10^4. These restrictions are more extensive than those used in previous calculations[40,41] but are required by the low symmetry, the application of electric fields, and the large number of excited states required; a consequence of this is that the SAC-CI energy displays small but noticeable discontinuities as a function of the electric-field strength.

For CASPT2, an active space consisting of eight electrons in the four highest-energy occupied π orbitals and the four lowest-energy unoccupied π orbitals is used for all calculations involving applied electric fields; this active space is notated as $(n,m) = (8,8)$ when n is the number of active electrons and m is the number of active orbitals. This is smaller than that which is required to achieve the good agreement between calculated and observed transition energies that is characteristic for this method[1,38,43] and is smaller than the (12,12) active space used in the most previous calculations on porphyrin.[38] Even the (12,12) active space is too small to quantitively describe all of the high-energy states of relevance herein, however, and so we also perform a (16,15) calculation to understand the relevant shortcomings of the (8,8) active space. This expanded calculation includes the 8 highest-energy occupied π orbitals and the 7 lowest-energy unoccupied π orbitals in the active space.

TABLE 1: Electronic Vertical Transition Energies *E* (in eV), Oscillator Strengths *f*, and Dominant Orbital Excitations for Free-Base Porphyrin

				observed			CAM-B3LYP 6-31G*		SAC-CI 6-31G*		SAC-CI 6-31G		CASPT2(8,8)[f] 6-31G		CASPT2(16,15) 6-31G	
symmetry	state	orbitals	CT[a]	ΔE	ΔE[d]	f[e]	ΔE	f	ΔE	f	ΔE	f	ΔE^x	ΔE^y	ΔE	f
B_{3u}	Q_x	$5b_{1u} \rightarrow 4b_{2g}$, $2a_u \rightarrow 4b_{3g}$	n	1.98−2.02[b]	1.91	0.01	2.19	0.001	1.71	0.003	1.80	0.0001	1.83	1.57	1.84	0.0016
B_{2u}	Q_y	$5b_{1u} \rightarrow 4b_{3g}$, $2a_u \rightarrow 4b_{2g}$	n	2.33−2.42[b]	2.27	0.06	2.42	0.001	2.10	0.001	2.29	0.0005	2.30	2.35	2.24	0.0070
B_{3u}	B_x	$2a_u \rightarrow 4b_{3g}$, $5b_{1u} \rightarrow 4b_{2g}$	n	3.13−3.33[c]	∼2.97	1.15	3.55	0.81	3.46	1.00	3.62	1.10	3.33	3.16	3.56	0.98
B_{2u}	B_y	$2a_u \rightarrow 4b_{2g}$, $5b_{1u} \rightarrow 4b_{3g}$	n	3.13−3.33[c]	∼2.97	1.15	3.69	1.16	3.61	1.49	3.77	1.64	3.39	3.39	3.12	0.76
B_{1g}	N_{xy}	$3b_{3g} \rightarrow 4b_{2g}$	y	> 3.1			3.88		3.53		3.71		4.00	3.73	3.88	
B_{3u}	N_x	$4b_{1u} \rightarrow 4b_{2g}$	y	3.65[e]	∼3.4	<0.1	4.28	0.59	4.09	0.89	4.22	0.85	3.91	3.71	3.72	0.025
A_g	N_s	$3b_{3g} \rightarrow 4b_{3g}$	y				4.38		4.00		4.14		3.63	3.50	3.91	
B_{2u}	N_y	$4b_{1u} \rightarrow 4b_{3g}$	y	3.65[e]	∼3.4	<0.1	4.50	0.073	4.19	0.36	4.39	0.27	3.73	3.67	3.95	0.51
A_u	(n,π^*)	$17b_{2u} \rightarrow 4b_{2g}$	y				4.57		4.35		4.25					
B_{2g}	(n,π^*)	$20a_g \rightarrow 4b_{2g}$	n				4.57		4.32		4.21					
B_{3g}	(n,π^*)	$20a_g \rightarrow 4b_{3g}$	y				4.75		4.45		4.43					
B_{1u}	(n,π^*)	$17b_{2u} \rightarrow 4b_{3g}$	n				4.76	0.003	4.50	0.003	4.49					
B_{1g}		$3b_{2g} \rightarrow 4b_{3g}$	y				4.76		4.36		4.72		3.31	3.42	4.23	
B_{1g}		$5b_{1u} \rightarrow 3a_u$	y				4.87				4.42		3.19	2.68	3.88	
A_g		$2a_u \rightarrow 3a_u$	n				4.87		4.44		4.59		3.94	3.74	4.50	

[a] State predicted to readily break symmetry and gain significant charge-transfer (CT) character: y = yes, n = no. [b] Gas phase and various solvents, from refs 36, 67, and 68. [c] Gas phase and various solvents, from refs 36, 68, and 69. [d] In light petroleum, from ref 38, for tetrameso-substituted porphyrin. [e] Gas phase, from ref 36. [f] Separate calculations for *x* and *y* polarized states.

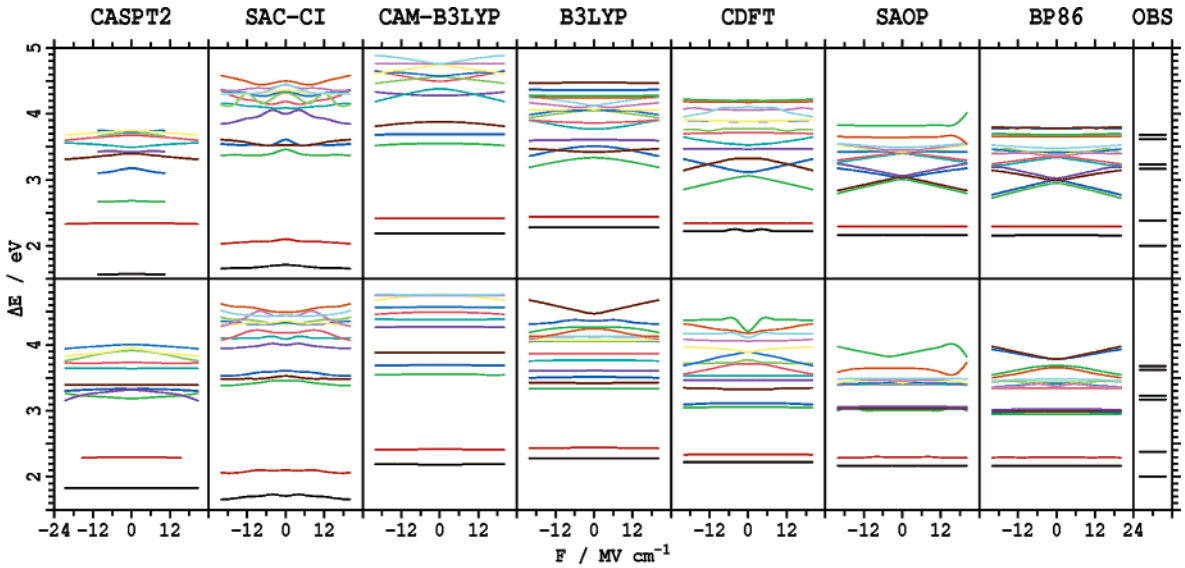

Figure 3. Calculated effects of in-plane *x* (lower panels) and *y* (upper panels) electric fields on the transition energies of porphyrin, compared to the observed (Table 1) field-free vertical excitation energies.

Significantly, the (8,8) active space is sufficient to provide basic continuity as a function of in-plane electric fields of up to 15−20 MV cm^{-1}. In addition, state averaging of the CASSCF wave functions must be specified, and as the nature of the states that mix changes depending on whether the electric field is applied in the *x*- or *y*-directions, two independent estimates of the field-free transition energies actually result. With the (8,8) active space we determine the energies for the lowest 15 states in each of the two (π,π^*) symmetries at finite fields, with relative weights in the CASSCF step of 1, 1, 1, 1, 1, 1, 1, 1, 0.8, 0.6, 0.4, 0.2, 0, 0, and 0 so as to reduce discontinuities associated with changes in the nature of the included states with increasing field strength. With the (16,15) active space, we include only three states of each symmetry and use an equal weighting for all states.

3. Results for the Porphyrins

The observed spectra[38] for P, P_1TA, and P_2TA are shown in Figure 2, along with stick representations of the calculated spectra obtained using the B3LYP, BP86, SAOP, CDFT, and CASPT2[38] methods. In this figure a color code is used to indicate assignment, blue for the Q-bands, red for the Soret bands, purple for the N-bands, green for the porphyrin-to-TA-bridge (P → B) charge-transfer bands, and black for calculated bands typically of a charge-transfer nature that cannot be readily related to observed ones. As has been previously shown,[38] the CASPT2 results are in good qualitative agreement with the experimental spectra, though quantitative accuracy is limited by the practical restrictions required for the application of this method to molecules the size of porphyrin dimers. They reflect the basic Gouterman model for porphyrinic spectra, supplemented with the N-band transitions as well as new P → B transitions associated with the fusion of the TA unit to the porphyrin. Similar good qualitative agreement is also found between experiment and the CAM-B3LYP results.

In contrast, the other density functionals B3LYP, BP86, SAOP, and CDFT all predict that the N-bands lie between the Q and Soret bands of P as well as extremely large numbers of accessible states for P_1TA and P_2TA; this scenario is the same as that found previously[38] for other density functionals and is qualitatively inconsistent with the experimental data. Note that the spectra calculated for BP86 using Gaussian with the 6-31G*

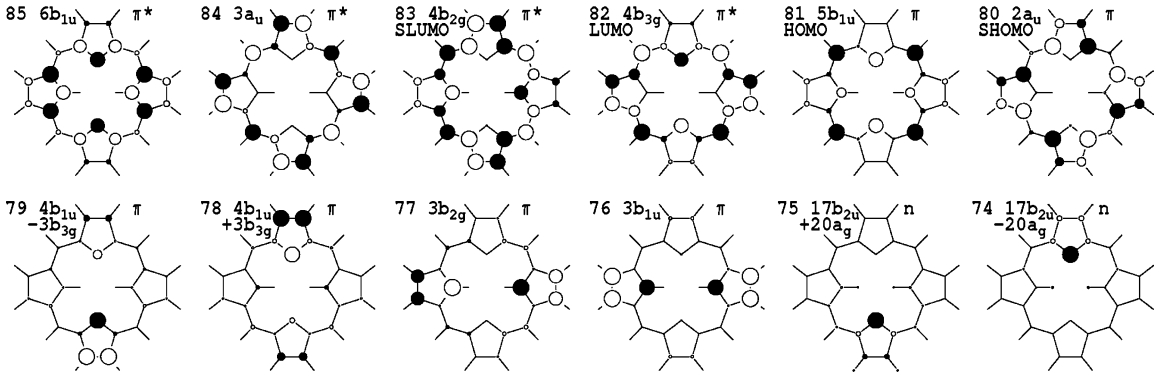

Figure 4. Orbital diagrams indicating the composition of some key n, π, and π^* orbitals of porphyrin at an applied field of 5.1 MV cm^{-1} (0.001 au) in the *y* (vertical) direction, as calculated by CAM-B3LYP. This field is sufficient to completely mix (b_{1u},b_{3g}) or (b_{2u},a_g) orbital pairs that are not delocalized over all four pyrrole rings and hence localize orbitals on single pyrroles, hence introducing the possibility of intramolecular inter-ring charge-transfer processes.

basis set and using ADF with the very much more extensive TZP basis set are essentially equivalent, confirming earlier observations[38,42] that basis set expansion beyond double-ζ is not critical for determining porphyrin valence spectra; quantitatively, however, basis set expansion beyond 6-31G* appears to reduce most calculated energy levels by ca. 0.1 eV and hence provide improved agreement with the experimental data.

The observed transition energies and oscillator strengths for free-base porphyrin and its tetrameso derivative[38] are given in Table 1 along with those calculated for free-base porphyrin using CAM-B3LYP, SAC-CI, CASPT2(8,8), and CASPT2(16,15), while calculated values from B3LYP, BP86, SAOP, and CDFT are provided in the Supporting Information. The close analogy between the observed spectra of the substituted and unsubstituted free-base porphyrin confirm that the substitution has minimal influence. The results shown for SAC-CI using the 6-31G* and 6-31G basis sets closely parallel those previously obtained using similar basis sets[39−41] as well as those obtained using the analogous STEOM-CC method;[44] improvement in basis set lowers the calculated transition energies by typically 0.1−0.2 eV, with the Q_y transition energy being the most sensitive. For most bands, the CAM-B3LYP, SAC-CI, and CASPT2(16,15) predictions are in good semiquantitative agreement with each other, with experiment, and with previous multireference configuration interaction[46,47] and CASPT2[12,38,42,43] calculations. For the low-energy Q-bands the agreement is very good indeed, but the disparities increase with increasing transition energy with the energies appearing typically in the pattern: observed < CASPT2(16,15) < SAC-CI < CAM-B3LYP. The seemingly more accurate results for CASPT2(16,15) may be due to the significant contribution of double and higher excitations to these transitions, excitations that are not as well represented in SAC-CI and TD-DFT calculations as are standard single excitations. For our purposes, the most significant feature of these results is that all computational methods lead to the same basic qualitative interpretation and assignment of the spectra of porphyrin. The less accurate CASPT2(8,8) calculations are also in good qualitative agreement with the other methods except for the supposedly highest-energy B_{1g} and A_g states. For these, the restricted active space leads to underestimation of the transition energies compared to CASPT2(16,15) by up to 1.2 eV.

The general natures of the low-lying excited states of porphyrin are summarized in Table 1 in terms of the principal orbital excitations involved in the transitions (Slightly perturbed variants of these orbitals are shown later in Figure 4.) The four lowest-energy transitions, Q_x, Q_y, B_x, and B_y are readily described in terms of excitations among the highest-occupied molecular orbital (HOMO) $5b_{1u}$, the second-highest-occupied molecular orbitals (SHOMOs) $2a_u$, the lowest-unoccupied molecular orbital (LUMO) $4b_{3g}$, and the second-lowest-unoccupied molecular orbital (SLUMO) $4b_{2g}$. Next follow another set of four states that we describe as N_{xy}, N_x, N_s, and N_y; of these, N_x and N_y are the well-known allowed N-band excitations of B_{3u} and B_{2u} symmetry arising from transitions from the third-highest-occupied molecular orbital $4b_{1u}$ to the LUMO and SLUMO. However, $4b_{1u}$ is nearly degenerate with an orbital of similar composition, $3b_{3g}$, and the excitations from this to the LUMO and SLUMO, of symmetries B_{2g} and A_g, respectively, combine to form the second four-state set. We call these transitions N_{xy} and N_s to reflect their *xy* and (x^2, y^2, z^2) symmetries, respectively. A third set of four states is also found, these arising from (n,π^*) excitations from the nitrogen lone-pair orbitals n to the LUMO and SLUMO.

Shown in Figure 3 are the effects of the application of in-plane polarized electric-field strengths (of magnitude on the order of the fields created naturally inside photosynthetic proteins[56]) on the calculated electronic absorption energies of porphyrin as well as the observed field-free state energies from Table 1. SAC-CI and CAM-B3LYP are clearly seen to overestimate the Q−Soret splitting in porphyin. The gap between the Q-bands and the next states is significantly reduced by B3LYP and more so by CDFT, SAOP, and BP86, but for these methods the next states are shown to respond significantly to applied electric fields, thus readily breaking symmetry to attain the significant dipole moments characteristic of charge-transfer bands. These states are not the expected Soret bands, the Soret bands becoming meshed within the charge-transfer excited-state manifold. This scenario is the same as that known already[13,55] for chlorophylls.

Inspection of the calculated field dependences from SAC-CI and CAM-B3LYP indicates that many of the states of higher energy than the Soret band are predicted to be charge-transfer states. On the basis of this analysis, all states in Table 1 are labeled as to whether they are dominated by charge-transfer character. While the Gouterman Q and Soret bands are not charge-transfer bands, the majority of other transitions, including the N-bands and the (n,π^*) bands, are. Despite the lack of quantitative accuracy in the CASPT2 finite-field calculations also shown in the figure, it is clear that this method predicts the same basic scenario. The intrinsic charge-transfer nature of the N and higher bands has not previously been recognized, though these bands are known to show significant solvent dependence.

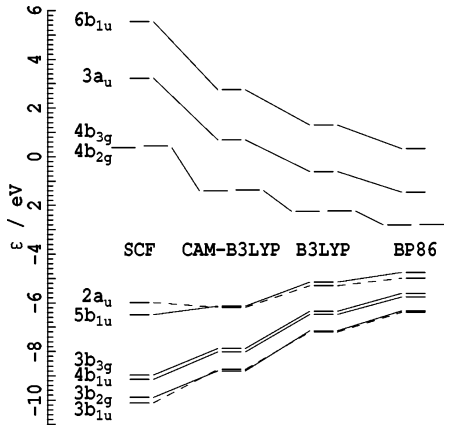

Figure 5. Calculated energies for some key porphyrin π and π^* orbitals.

The calculated spectral properties can be understood in terms of the nature of the key prophyrin orbitals, shown in Figure 4, and the variation of their energies with computational method, shown in Figure 5. A key characteristic of the four orbitals used in the Gouterman model, the SHOMO, HOMO, LUMO, and SLUMO, is that they are delocalized over all four pyrrole rings. Many other occupied orbitals, including $3b_{3g}$ and $4b_{1u}$ shown in Figure 4, are delocalized over just two of the four rings; however, the nodes on the intermediary rings indicate that there is very little electronic interaction between the opposing rings. For these orbitals, the application of weak electric fields in the direction between the two participating pyrroles breaks the symmetry and causes the orbitals to localize on single rings. This is demonstrated in Figure 4 where an applied field strength of 5 MV cm^{-1} in the *y*-direction is shown to completely mix $4b_{1u}$ with $3b_{3g}$ to produce localized orbitals; a similar effect is also seen for the lone-pair (n) orbitals $17b_{2u}$ and $20a_g$. Excitations involving localized orbitals create inter-pyrrole charge transfer and give rise to the linear Stark effects depicted in Figure 3 for field-strength magnitudes above the critical value (typically <1 MV cm^{-1}) required to break symmetry. All four transitions in the N-band set are thus intrinsically of a charge-transfer nature and are mixed together very strongly by weak external electric fields. They must be taken as an entity when considering the non-Gouterman spectroscopy of porphyrin. Geometrical distortions will also strongly mix the four N-band components, giving rise to strong vibronic coupling and intensity sharing. Finally, chemical substitutions that lower the symmetry of the prophyrin are also expected to strongly mix these components, redistributing the allowed N-band intensity among all four components. An example of this effect, as discussed in detail in the next section, is Chl a; P_1TA provides another example, with the analogous $4b_{1u}$ and $3b_{3g}$ pyrrole orbitals automatically localizing, one of these then delocalizing into the TA bridge so as to confuse the nature of the N-bands in this molecule with bridge-to-porphyrin transitions. Hence, while the Gouterman Q and Soret bands take similar forms in all porphyrin-type macrocycles, the non-Gouterman transitions are very sensitive to the chemical environment.

Figure 5 shows that, while the failure of BP86 and other traditional density functionals to predict the spectra of oligoporphyrins is dramatic, the origin of the effect arises from subtle inadequacies in calculated orbital energies rather than from catastrophic failure of the methodology. As is well-known, BP86, etc. predict rather small HOMO−LUMO gaps; Figure 5, however, shows that the spacings *within* the occupied and virtual manifolds are also much smaller than those predicted by other methods such as the Hartree−Fock self-consistent field (SCF). The SCF HOMO−LUMO band gap reflects primarily the energies of ion formation whereas the BP86 energies primarily reflect the much smaller HOMO−LUMO excitation energy. Through the use of both approaches, proper formalisms treating the occupied and virtual bands have been developed for the accurate prediction of both the ion formation and the excitation energies; as a result, all methods predict realistic values of the porphyrin Q-band energies *irrespective* of their intrinsic HOMO−LUMO gap. However, the contraction *within* the occupied and virtual bands evident in Figure 4 cannot be readily accounted for, and as a result the energy differences calculated by traditional density functionals between the HOMO−LUMO excited state and the others (especially those involving charge transfer) decrease alarmingly.

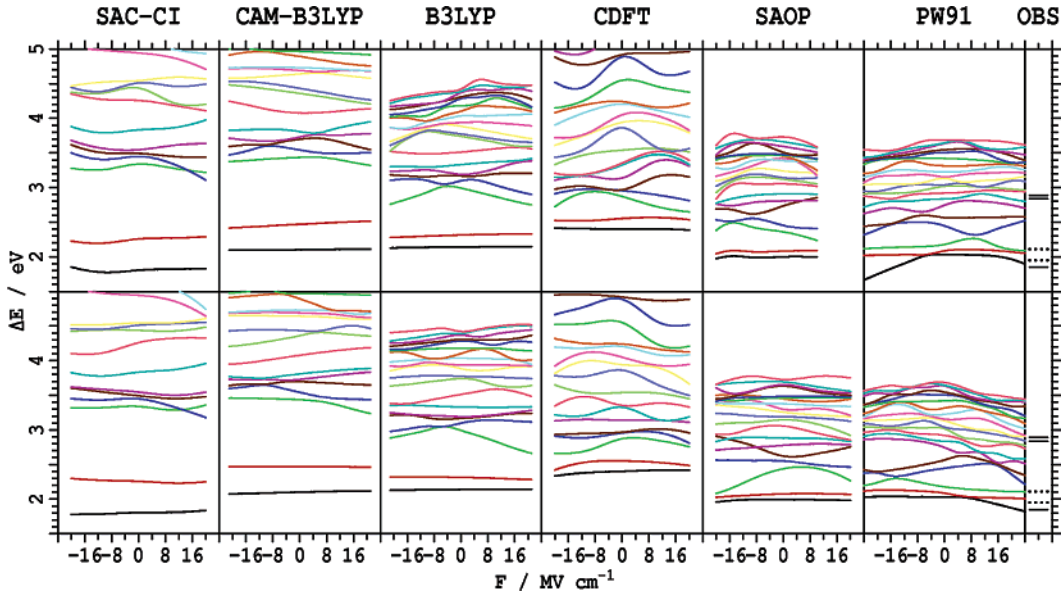

Figure 6. Calculated effects of in-plane *x* (lower panels) and *y* (upper panels) electric fields on the transition energies of chlorophyll a, compared to the observed (Table 2) field-free vertical excitation energies. (The alternate possibilities for the assignment of Q_x are shown as dotted lines.)

TABLE 2: Calculated and Observed Vertical Excitation Energies (in eV), Oscillator Strengths *f*, Polarization Angles (in deg in the Coordinate System of Fragata et al.[50] Shown in Figure 7), and Dominant Orbital Excitations (Figure 7) for Chlorophyll a

			observed[a]		CAM-B3LYP 6-31G*			SAC-CI 6-31G*			SAC-CI 6-31G		
state	orbitals	CT	ΔE	pol.	ΔE	f	pol.	ΔE	f	pol.	ΔE	f	pol.
Q_y	166 → 167, 165 → 168	n	1.85[b]	70	2.10	0.24	78	1.75	0.29	74	1.81	0.22	75
Q_x	165 → 167, 166 → 168	n	1.95/2.11[cd]	0	2.47	0.026	25	2.26	0.018	15	2.26	0.026	6
B_x	166 → 168, 165 → 167	n	2.84[d]	0	3.44	0.79	−7	3.30	1.00	−2	3.34	1.03	9
$N_x + N_{xy}$	164 → 167	y			3.54	0.30	29	3.53	0.42	−22	3.55	0.17	−14
B_y	165 → 168, 166 → 167	n	2.9−3.3[d]	90	3.70	0.81	78	3.52	0.69	85	3.49	0.87	83
(O_n,π^*)	161 → 167	y			3.73	0.072	91				4.51	0.001	73
$L_x + L_{xy}$	163 → 167	y			3.81	0.018	75	3.40	0.075	−46	3.45	0.080	−46
$N_x - N_{xy}$	162 → 167	y			4.08	0.16	−19	3.79	0.038	45	3.83	0.032	−20
$L_y + L_s$	163 → 168	y			4.36	0.092	77				4.26	0.112	40
	166 → 169	y			4.43	0.051	5						
	160 → 167	n			4.64	0.036	34	4.55	0.096	82	4.44	0.125	62
	165 → 169	n			4.69	0.165	−74				5.09	0.32	−76
	157 → 167	y			4.73	0.003	76						
$N_y + N_s$	164 → 168	y			4.89	0.058	72				4.94	0.015	13
	159 → 167	n			4.97	0.078	−43				4.55	0.064	−39
$N_y - N_s$	162 → 168	y									5.26	0.038	82

[a] In a liquid crystal of glycerylmonooctanoate/H_2O from ref 50. [b] Observed in ether[52] at 1.88 eV, extrapolated to the gas phase[64] at 1.91 eV. [c] Two absorption bands observed[50] at 1.95 eV (latest assignment[52]) and 2.11 eV (traditional assignment) corresponding to bands observed by magnetic circular dichroism in ether[52] at 2.01 and 2.15 eV, respectively. [d] Increases of ca. 0.1 eV are naively expected for these transitions in the gas-phase based on known solvent susceptibilities.[52,64,65]

4. Results for Chlorophyll a

It has previously been shown that DFT calculations using traditional functionals such as BP86 and PW91 predict charge-transfer states within the Q−B gap[55] whose electric-field responses are qualitatively inconsistent with known properties of chlorophylls in plants.[13] An example of results exemplifying this is given in Figure 6, depicting the calculated electric-field responses[13] for PW91. Results for more modern approaches attempting to address the basic failures of traditional density functions are also included in this figure: The SAOP, CDFT, and B3LYP functionals make improvements but clearly remain inadequate, while only CAM-B3LYP predicts the key experimentally observed feature of distinct Q and Soret bands. Results from SAC-CI calculations are also included in the figure and appear qualitatively very similar to those from CAM-B3LYP. As found in the previous section for porphyrin, charge-transfer bands are inherent to the spectroscopy of chlorophylls, with again the N-bands predicted to be of charge-transfer character. However, the Q- and B-bands show more enhanced susceptibilities to external electric fields for chlorophylls than for porphyrins, reflecting the observed enhanced solvent shifts of the transition energies;[52,64,65] see Tables 1 and 2.

Quantitative predictions for Chl a obtained using CAM-B3LYP and SAC-CI are given in Table 2 while results from B3LYP, SAOP, and CDFT are provided in the Supporting Information. For SAC-CI, results obtained using the 6-31G* and 6-31G basis sets are included, these being very similar to each other and to previous SAC-CI results obtained using similar basis sets.[41] Shown in the table are both the band assignments made on the basis of the orbitals involved in each excitation combined with the calculated transition-moment polarization direction and an assignment of each band as predominantly charge transfer or not based on the electric-field responses shown in Figure 6. For the low-lying states, the CAM-B3LYP transition energies are 0.1−0.35 eV higher than the SAC-CI ones, the greatest difference being for the first excited stated Q_y. While these calculations, along with previous multireference configuration interaction ones,[45,46] exclude the possibility that the two bands observed[50,52] in the spectrum of Chl a at 1.95 and 2.11 eV both correspond to electronic-state origins, the lowest-energy charge-transfer state is predicted by both methods to be only ca. 0.1 eV greater in energy than B_x. There is thus the possibility of strong interaction of the Soret bands with charge-transfer transitions.

The general nature of the excited states of Chl a are found to be very similar to those for porphyrin, with the dominant orbitals involved in the transitions being shown in Figure 7 along with the (x,y) axis definitions. By comparison of Figures 4 and 7, it is clear that the SHOMO, HOMO, LUMO, and SLUMO orbitals of porphyrin and Chl a are very similar, but there is a significant splitting in the LUMO and SLUMO orbital energies for Chl a, and this reduces the interference between the excitations and hence allows more intensity into the Q_y band. There are striking qualitative differences between the orbitals that give rise to the N- and L-bands, however. For porphyrin, the N-bands arise from transitions from the $4b_{1u}$ and $3b_{3g}$ orbital pair while the L-bands arise from transitions from the analogous $3b_{1u}$ and $3b_{2g}$ pair; all four orbitals share the same parentage in terms of localized pyrrole contributions in metalloporphyrins. These orbitals are delocalized in high-symmetry environments but, as shown in Figure 4, become mixed to form orbitals localized on the individual pyrrole rings upon application of weak external electric fields. However, Figure 7 indicates that these transitions are *intrinsically localized* on individual pyrrole rings in Chl a. In Table 2, the N-bands are described as the linear combinations $N_x \pm N_{xy}$ and $N_y \pm N_s$ to reflect this fundamental difference in the nature of these bands in porphyrins and chlorophylls, indicating explicitly how the forbidden N-band components in porphyrin become allowed in Chl a. Also indicated in Figure 7 is that, because of the chlorin modification to the ring system that hydrogenates one of the $C_\beta-C_\beta$ bonds, only three localized pyrrole orbitals exist (numbers 162−164 in Figure 7) instead of four (numbers 76−79 in Figure 4). The result is that only two mixed L components exist instead of four, named $L_x + L_{xy}$ and $L_y + L_x$ in Table 2, and these components move to lower energy than would otherwise be expected. Also, the chlorophyl LUMO−SLUMO energy gap introduces significant splitting between the N_{xy}/N_s and N_x/N_y pairs, placing the L-bands within the N-band manifold. The situation found for P_1TA is very similar to this.

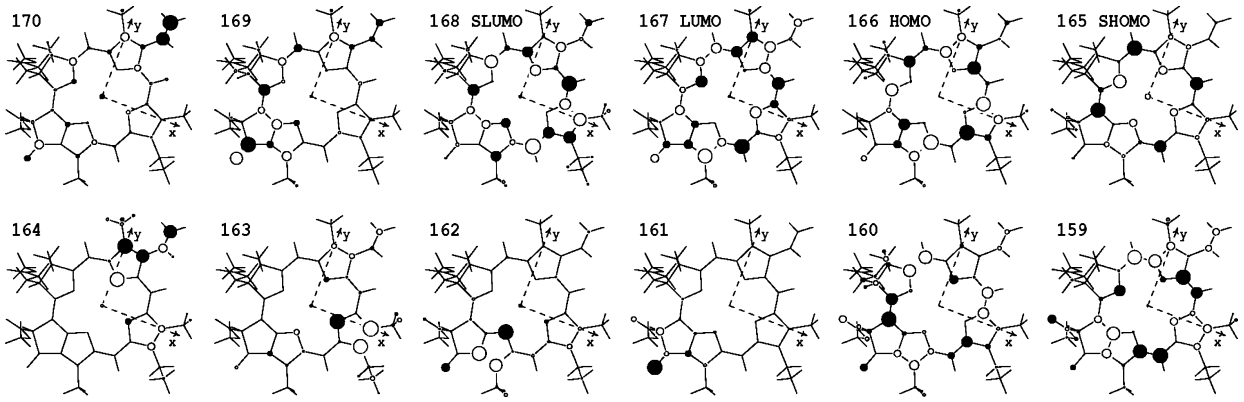

Figure 7. CAM-B3LYP orbital diagrams indicating the composition of some key orbitals of chlorophyll a, including the axis definitions of Fragata et. al.[50] The orbital localization that is induced by small fields in porphyrin is intrinsic to this molecule.

Another significant difference between Chl a and P is that the (n,π^*) bands originating from the nitrogen lone pairs in porphyrin no longer exist, while new lone-pair transitions (O_n,π^*) involving the carbonyl groups are introduced. Interestingly, the largest difference between the CAM-B3LYP and the SAC-CI results occurs for this state, an explicitly charge-transfer state that CAM-B3LYP underestimates by 0.8 eV compared to SAC-CI. This is contrary to the general trend of CAM-B3LYP predicting higher energies than SAC-CI, and hence it is clear that molecular processes of this type warrant further investigations into the reliability of these computational methods.

5. Conclusions

The underestimation of band gaps by traditional density functions is well-known. Typically, this has little effect on ground-state properties, however, with low calculated reaction barrier heights being a known significant consequence. When the band gap narrows too much or disappears, profound ramifications occur, however. Systems to which this scenario is apt include conducting polymers, molecular electronics, and chemical or biological electron and energy transfer devices, systems with many applications in nanotechnology and biotechnology. B3LYP was an early functional designed to combat these problems, increasing band gaps through the inclusion of nonlocal Hartree−Fock exchange into the functional. The success of B3LYP in achieving this is demonstrated in Figure 5 where the calculated band gap for porphyrin is significantly enhanced compared to that calculated by BP86, with Figures 3 and 6 showing significantly improved spectroscopic predictions for porphyrin and Chl a. However, as Figure 2 shows, this improvement is insufficient to provide a proper description for extended conjugated systems such as oligoporphyrins, and like the traditional GGAs, B3LYP fails to predict a singlet ground state for polyacetylene.[38] Also, the combination in B3LYP of nonlocal exchange with the local correlation functions used in GGAs results in some bizarre behavior for the interaction of open-shell systems at long distance, systems that are paradigms for single-molecule conductivity.[66] CAM-B3LYP provides an improvement to B3LYP in which nonlocal exchange is damped outside of interatomic interaction distances, providing a better match with local correlation functionals. This provides a more correct asymptotic behavior for charge-transfer transitions. It opens the HOMO−LUMO gap to prevent molecules from being perceived by DFT as having metallic character.

A variety of other methods have been developed to provide long-range corrections to density functionals, and herein we considered the SAOP GGA and the CDFT. Both were found to be inadequate for the description of extended conjugation in porphyrins and chlorophylls. Current-density functionals build into the Hamiltonian realistic descriptions of both the very short-range correlation and the very long-range correlation, with the hope that correlation on the intermediate length scales of atomic bonds and molecular dimensions would be well represented. Our results indicate that further revision of this type of density functional is required before they can be robust functions for use in nanotechnological and biotechnological applications involving electron and energy transport through conjugated systems.

While the accuracy of the methods employed herein is found to be in the order CASPT2(16,15) > SAC-CI > CAM-B3LYP > CASPT2(8,8) ≫ B3LYP > CDFT > SAOP > BP86 and PW91, the computational resources required scale as SAC-CI > CASPT2(16,15) > CDFT ≫ CASPT2(8,8) ≫ CAM-B3LYP > B3LYP > SAOP, BP86, and PW91, with the CASPT2 calculations requiring by far the most human control and expertise to perform. CAM-B3LYP thus provides an easy to use, cost-efficient method for obtaining practicable accuracy for properties of charge-transfer systems.

While it is known that traditional density functionals erroneously predict the occurrence of charge-transfer bends between the Q and Soret bands of chlorophylls,[38,55] the results obtained here for CAM-B3LYP and for SAC-CI confirm that charge-transfer bands are significant in chlorophyll spectroscopy but are located near or above the Soret bands. Further, these methods as well as CASPT2 predict that charge-transfer bands are of generic importance for porphyrins but again are located above the Soret band in free-base porphyrin. In particular, the N-bands of porphyrins and chlorophylls are shown to be charge-transfer bands. Porphyrin orbitals are shown to be of two generic types, those like the well-known four Gouterman orbitals that are completely delocalized over all four pyrrole rings and others that are located on only two opposing rings; these latter orbitals are shown to readily localize under external perturbations, giving rise to many intramolecular charge-transfer processes that make the non-Gouterman transitions very sensitive to chemical environment.

Acknowledgment. We thank the Australian Research Council for funding this work, the Australian Partnership of Advanced Computing for provision of computational resources, and Dr. M. Frisch from Gaussian, Inc., for access to the development version of Gaussian. Some of the calculations used Primepower supplied by Fujitsu, Japan.

Supporting Information Available: Calculated DFT electronic transition properties of free-base porphyrin and chloro-

phyll a. This material is available free of charge via the Internet at http://www.acs.org/.

References and Notes

(1) Tozer, D. J.; Amos, R. D.; Handy, N. C.; Roos, B. O.; Serrano-Andres, L. *Mol. Phys.* **1999**, *97*, 859.

(2) Dreuw, A.; Head-Gordon, M. *Chem. Rev.* **2005**, *105*, 4009.

(3) Bauernschmitt, R.; Ahlrichs, R. *Chem. Phys. Lett.* **1996**, *256*, 454.

(4) Casida, M. E.; Casida, K. C.; Salahub, D. R. *Int. J. Quantum Chem.* **1998**, *70*, 933.

(5) Casida, M. E.; Jamorski, C.; Casida, C. K.; Salahub, D. R. *J. Chem. Phys.* **1998**, *108*, 4439.

(6) Casida, M. E.; Gutierrez, F.; Guan, J.; Gadea, F.-X.; Salahab, D.; Daudey, J.-P. *J. Chem. Phys.* **2000**, *113*, 7062.

(7) Jamorski, C.; Casida, M. E.; Salahab, D. R. *J. Chem. Phys.* **1996**, *104*, 5134.

(8) Dreuw, A.; Head-Gordon, M. *J. Am. Chem. Soc.* **2004**, *126*, 4007.

(9) Gritsenko, O. V.; Schipper, P. R. T.; Baerends, E. J. *Chem. Phys. Lett.* **1999**, *302*, 199.

(10) Tozer, D. J.; Handy, N. C. *J. Chem. Phys.* **1998**, *109*, 10180.

(11) Spielfiedel, A.; Handy, N. C. *Phys. Chem. Chem. Phys.* **1999**, *1*, 2383.

(12) Cai, Z.-L.; Sendt, K.; Reimers, J. R. *J. Chem. Phys.* **2002**, *117*, 5543.

(13) Dahlbom, M. G.; Reimers, J. R. *Mol. Phys.* **2005**, *103*, 1057.

(14) Champagne, B.; Perpáte, E. A.; van Gisbergen, S. J. A.; Baerends, E. J.; Snijders, J. D.; Soubra-Ghauoi, C.; Robins, K. A.; Kirtman, B. *J. Chem. Phys.* **1998**, *109*, 10489.

(15) van Gisbergen, S. J. A.; Schipper, P. R. T.; Gritensko, O. V.; Baerends, E. J.; Snijders, J. D.; Champagne, B.; Kirtman, B. *Phys. Rev. Lett.* **1999**, *83*, 694.

(16) de Boeij, P. L.; Kootstra, F.; Berger, J. A.; van Leeuwen, R.; Snijders, J. G. *J. Chem. Phys.* **2001**, *115*, 1995.

(17) Reimers, J. R.; Cai, Z.-L.; Bilic, A.; Hush, N. S. *Ann. N. Y. Acad. Sci.* **2003**, *1006*, 235.

(18) Tozer, D. J. *J. Chem. Phys.* **2000**, *112*, 3507.

(19) Wu, Q.; Ayers, P. W.; Yang, W. *J. Chem. Phys.* **2003**, *119*, 2978.

(20) Tawada, Y.; Tsuneda, T.; Yanagisawa, S.; Yanai, T.; Hirao, K. *J. Chem. Phys.* **2004**, *120*, 8425.

(21) van Leeuwen, R.; Baerends, E. J. *Phys. Rev. A* **1994**, *49*, 2421.

(22) Cai, Z.-L.; Tozer, D. J.; Reimers, J. R. *J. Chem. Phys.* **2000**, *113*, 7084.

(23) Schipper, P. R. T.; Gritsenko, O. V.; van Gisbergen, S. J. A.; Baerends, E. J. *J. Chem. Phys.* **1999**, *112*, 1344.

(24) van Faassen, M.; de Boeij, P. L.; van Leeuwen, R.; Berger, J. A.; Snijders, J. G. *J. Chem. Phys.* **2003**, *118*, 1044.

(25) Yanai, T.; Tew, D. P.; Handy, N. C. *Chem. Phys. Lett.* **2004**, *393*, 51.

(26) Becke, A. D. *J. Chem. Phys.* **1993**, *98*, 5648.

(27) Stephens, P. J.; Devlin, F. J.; Chabalowski, C. F.; Frisch, M. J. *J. Phys. Chem.* **1994**, *98*, 11623.

(28) van Faassen, M.; de Boeij, P. L. *J. Chem. Phys.* **2004**, *120*, 8353.

(29) Ullrich, C. A.; Burke, K. *J. Chem. Phys.* **2004**, *121*, 28.

(30) Peach, M. J. G.; Helgaker, T.; Salek, P.; Keal, T. W.; Lutnaes, O. B.; Tozer, D. J.; Handy, N. C. *Phys. Chem. Chem. Phys.* **2006**, *8*, 558.

(31) Kobayashi, R.; Amos, R. D. *Chem. Phys. Lett.* **2006**, *420*, 106.

(32) Perdew, J. P.; Zunger, A. *Phys. Rev. B* **1981**, *23*, 5048.

(33) Perdew, J. P. *Phys. Rev. B* **1986**, *33*, 8822.

(34) Perdew, J. P.; Wang, Y. *Phys. Rev. B* **1992**, *45*, 13244.

(35) Gouterman, M. *J. Mol. Spectrosc.* **1961**, *6*, 138.

(36) Edwards, L.; Dolphin, D. H.; Gouterman, M.; Adler, A. D. *J. Mol. Spectrosc.* **1971**, *38*, 16.

(37) Hush, N. S.; Dyke, J. M.; Williams, M. L.; Woolsey, I. S. *J. Chem. Soc., Dalton Trans.* **1974**, *4*, 395.

(38) Sendt, K.; Johnston, L. A.; Hough, W. A.; Crossley, M. J.; Hush, N. S.; Reimers, J. R. *J. Am. Chem. Soc.* **2002**, *124*, 9299.

(39) Nakatsuji, H.; Hasegawa, J.; Hada, M. *J. Chem. Phys.* **1996**, *104*, 2321.

(40) Tokita, Y.; Hasegawa, J.; Nakatsuji, H. *J. Phys. Chem. A* **1998**, *102*, 1843.

(41) Hasegawa, J.; Ozeki, Y.; Ohkawa, K.; Hada, M.; Nakatsuji, H. *J. Phys. Chem. B* **1998**, *102*, 1320.

(42) Merchàn, M.; Ortí, E.; Roos, B. O. *Chem. Phys. Lett.* **1994**, *226*, 27.

(43) Serrano-Andrés, L.; Merchàn, M.; Rubio, M.; Roos, B. O. *Chem. Phys. Lett.* **1998**, *295*, 195.

(44) Gwaltney, S. R.; Bartlett, R. J. *J. Chem. Phys.* **1998**, *108*, 6790.

(45) Parusel, A. B. J.; Grimme, S. *J. Phys. Chem. B* **2000**, *104*, 5395.

(46) Parusel, A. B. J.; Grimme, S. *J. Porphyrins Phthalocyanines* **2001**, *5*, 225.

(47) Parusel, A. B. J.; Ghosh, A. *J. Phys. Chem. A* **2000**, *104*, 2504.

(48) Parusel, A. B. J.; Grimme, S. *J. Phys. Chem. B* **2000**, *104*, 5395.

(49) van Gisbergen, S. J. A.; Rosa, A.; Ricciardi, G.; Baerends, E. J. *J. Chem. Phys.* **1999**, *111*, 2499.

(50) Fragata, M.; Norden, B.; Kurucsev, T. *Photochem. Photobiol.* **1988**, *47*, 133.

(51) Nordén, B.; Fragata, M.; Kurucsev, T. *Aust. J. Chem.* **1992**, *45*, 1559.

(52) Umetsu, M.; Wang, Z.-Y.; Kobayashi, M.; Nozawa, T. *Biochim. Biophys. Acta* **1999**, *1410*, 19.

(53) Sundholm, D. *Chem. Phys. Lett.* **1999**, *302*, 480.

(54) Sundholm, D. *Chem. Phys. Lett.* **2000**, *317*, 545.

(55) Dreuw, A.; Fleming, G. R.; Head-Gordon, M. *J. Phys. Chem. B* **2003**, *107*, 6500.

(56) Canfield, P.; Dahlbom, M. G.; Reimers, J. R.; Hush, N. S. *J. Chem. Phys.* **2006**, *124*, 024301.

(57) Kjellberg, P.; He, Z.; Pullerits, T. *J. Phys. Chem. B* **2003**, *108*, 13737.

(58) te Velde, G.; Baerends, E. J. *J. Comput. Phys.* **1992**, *99*, 84.

(59) Baerends, E. J. *ADF2005.1*; SCM, Theoretical Chemistry, Vrije University: Amsterdam, 2005.

(60) Frisch, M. J.; Trucks, G. W.; Schlegel, H. B.; Scuseria, G. E.; Robb, M. A.; Cheeseman, J. R.; Montgomery, Jr. J. A.; Vreven, T.; Kudin, K. N.; Burant, J. C.; Millam, J. M.; Iyengar, S. S.; Tomasi, J.; Barone, V.; Mennucci, B.; Cossi, M.; Scalmani, G.; Rega, N.; Petersson, G. A.; Nakatsuji, H.; Hada, M.; Ehara, M.; Toyota, K.; Fukuda, R.; Hasegawa, J.; Ishida, M.; Nakajima, T.; Honda, Y.; Kitao, O.; Nakai, H.; Klene, M.; Li, X.; Knox, J. E.; Hratchian, H. P.; Cross, J. B.; Bakken, V.; Adamo, C.; Jaramillo, J.; Gomperts, R.; Stratmann, R. E.; Yazyev, O.; Austin, A. J.; Cammi, R.; Pomelli, C.; Ochterski, J. W.; Ayala, P. Y.; Morokuma, K.; Voth, G. A.; Salvador, P.; Dannenberg, J. J.; Zakrzewski, V. G.; Dapprich, S.; Daniels, A. D.; Strain, M. C.; Farkas, O.; Malick, D. K.; Rabuck, A. D.; Raghavachari, K.; Foresman, J. B.; Ortiz, J. V.; Cui, Q.; Baboul, A. G.; Clifford, S.; Cioslowski, J.; Stefanov, B. B.; Liu, G.; Liashenko, A.; Piskorz, P.; Komaromi, I.; Martin, R. L.; Fox, D. J.; Keith, T.; Al-Laham, M. A.; Peng, C. Y.; Nanayakkara, A.; Challacombe, M.; Gill, P. M. W.; Johnson, B.; Chen, W.; Wong, M. W.; Gonzalez, C.; Pople, J. A. *Gaussian Development Version*, revison D.02; Gaussian, Inc.: Wallingford CT, 2004.

(61) Andersson, K.; Barysz, M.; Bernhardsson, A.; Blomberg, M. R. A.; Carissan, Y.; Cooper, D. L.; Cossi, M.; Fleig, T.; Fülscher, M. P.; Gagliardi, L.; de Graaf, C.; Hess, B. A.; Karlström, G.; Lindh, R.; Malmqvist, P.-Å.; Neogrády, P.; Olsen, J.; Roos, B. O.; Schimmelpfennig, B.; Schütz, M.; Seijo, L.; Serrano-Andrés, L.; Siegbahn, P. E. M.; Stålring, J.; Thorsteinsson, T.; Veryazov, V.; Wierzbowska, M.; Widmark, P.-O. *Molcas*, version 5.2; Lund University: Lund, Sweden, 2001.

(62) Nakatsuji, H. *Chem. Phys. Lett.* **1979**, *67*, 329.

(63) Stratmann, R. C.; Scuseria, G. E.; Frisch, M. J. *J. Chem. Phys.* **1998**, *109*, 8218.

(64) Fiedor, L.; Stasiek, M.; Mysliwa-Kurdziel, B.; Strazalka, K. *Photosynth. Res.* **2003**, *78*, 47.

(65) Limantara, L.; Sakamoto, S.; Koyama, Y.; Nagae, J. *Photochem. Photobiol.* **1997**, *65*, 330.

(66) Solomon, G. C.; Reimers, J. R.; Hush, N. S. *J. Chem. Phys.* **2004**, *121*, 6615.

(67) Kim, B. F.; Bohandy, J. *J. Mol. Spectrosc.* **1978**, *73*, 332.

(68) Nagashima, U.; Takada, T.; Ohno, K. *J. Chem. Phys.* **1986**, *85*, 4524.

(69) Rimington, C.; Mason, S. F.; Kennard, O. *Spectrochim. Acta* **1958**, *12*, 65.